J|A|C|S
ARTICLES
Published on Web 09/29/2006

Glycine at the Pyrite−Water Interface: The Role of Surface Defects

Nisanth N. Nair,* Eduard Schreiner, and Dominik Marx

Contribution from the Lehrstuhl für Theoretische Chemie, Ruhr-Universität Bochum, 44780 Bochum, Germany

Received May 11, 2006; E-mail: nisanth.nair@theochem.ruhr-uni-bochum.de

Abstract: Ab initio molecular dynamics simulations were performed in order to study chemisorption, electronic properties, and desorption of glycine at wet pyrite surfaces focusing on the role of surface point defects. The change in the electronic structure and its influence on the chemical reactivity of the free FeS_2-(100) surface due to sulfur vacancies was studied in detail yielding several adsorption modes of glycine and water molecules. Energetically preferred adsorption modes were furthermore investigated in the presence of hot pressurized water mimicking "Iron Sulfur World" prebiotic conditions. The metadynamics Car−Parrinello technique was employed to map the free energy landscape including paths and barriers for desorption of glycine from such wet defective surfaces. The ubiquitous sulfur vacancies are found to increase the retention time of the adsorbed amino acid by many orders of magnitudes in comparison to the ideal pyrite−water interface. The importance of these findings in terms of a possible two-dimensional primordial chemistry on mineral surfaces is discussed.

1. Introduction

Obviously the question of how life emerged on Earth remains unanswered, even after making enormous advances in science and technology. This field experienced a revival after electric discharge experiments in a hypothetic prebiotic atmosphere in the early 1950s.[1,2] Many alternative ideas have been developed and stimulated innovative experiments in order to explain how organic molecules were first synthesized in a prebiotic "inorganic" environment and how they organized themselves to form biomolecules of contemporary complexity. Although the entire field is far from reaching consensus,[3,4] the "crêpes versus soup"[5] or "hot stones versus cold soup"[6] question, i.e., two-dimensional versus three-dimensional reaction scenarios involving confining mineral surfaces[7] instead of a dilute bulk solution as the reaction environment, is moving into the focus of much current work.[4−15] One of the most acclaimed hypotheses in this respect is the one suggested by Wächtershäuser,[16,17] which has been however controversially discussed[18−23] ever since.

Wächtershäuser proposes a chemo-autotrophic origin of life,[16,17] which has been called the "Iron Sulfur World" (ISW) scenario. The main assumption in the ISW scenario is that prebiotic reactions such as condensations of amino acids are catalyzed by iron−sulfur minerals located near deep sea hydrothermal vents, i.e., in a high temperature and high-pressure aqueous environment. Experimental support for the ISW scenario was brought in 1997, as activated acetic acid was generated in laboratory experiments by a carbon fixation route at conditions mimicking the assumed primordial environment.[24] Shortly later, in experiments modeling the hydrothermal environment more closely, peptides were synthesized by polymerization of amino acids on iron−nickel sulfides.[25] Following the ideas of their previous experiments, Huber and Wächtershäuser finally put forward a primordial peptide cycle with closely related anabolic and catabolic segments.[26] More recently, the Orgel group demonstrated[27] that such chemical reactions indeed are feasible and can be catalyzed by metal-sulfides. Furthermore, the Geophysical Lab group concluded,[28] based on CO insertion

(1) Miller, S. L. *Science* **1953**, *117*, 528.
(2) Bada, J. L.; Lazcano, A. *Science* **2003**, *300*, 745.
(3) Deamer, D. W.; Fleischaker, G. R., Eds. *Origins of Life: The Central Concepts*; Jones and Bartlett Publishers: Boston, U.S.A., 1994.
(4) Fry, I. *The Emergence of Life on Earth: A Historical and Scientific Overview*. Rutgers University Press: New Jersey, U.S.A., 2000.
(5) von Kiedrowski, G. *Nature* **1996**, *381*, 20.
(6) Severin, K. *Angew. Chem., Int. Ed.* **2000**, *39*, 3589.
(7) Bernal, J. D. *The Physical Basis of Life*; Routledge and Kegan Paul: London, 1951.
(8) Hazen, R. M. *Sci. Am.* **2001**, *284*, 76.
(9) Kreisel, G.; Wolf, C.; Weigand, W.; Dörr, M. *Chem. Unserer Zeit* **2003**, *37*, 306.
(10) Saladino, R.; Crestini, C.; Costanzo, G.; DiMauro, E. *Curr. Org. Chem.* **2004**, *8*, 1425.
(11) Schoonen, M.; Smirnov, A.; Cohn, C. *Ambio* **2004**, *33*, 539.
(12) Plankensteiner, K.; Reiner, H.; Rode, B. M. *Origins Life Evol. Biospheres* **2005**, *35*, 411.
(13) Hazen, R. M. *Elements* **2005**, *1*, 135.
(14) Cody, G. D. *Elements* **2005**, *1*, 139.
(15) Smith, J. V. *Elements* **2005**, *1*, 151.
(16) Wächtershäuser, G. *Microbiol. Rev.* **1988**, *52*, 452.
(17) Wächtershäuser, G. *Prog. Biophys. Mol. Biol.* **1992**, *58*, 85.
(18) Duve, C. D.; Miller, S. L. *Proc. Natl. Acad. Sci. U.S.A.* **1991**, *88*, 10014.
(19) Cody, G. D.; Boctor, N. Z.; Filley, T. R.; Hazen, R. M.; Scott, J. H.; Sharma, A.; Yoder, H. S., Jr. *Science* **2000**, *289*, 1337.
(20) Wächtershäuser, G. *Science* **2000**, *289*, 1307.
(21) Bada, J. L.; Lazcano, A. *Science* **2002**, *296*, 1982.
(22) Wächtershäuser, G. *Science* **2002**, *298*, 748.
(23) Hagmann, M. *Science* **2002**, *295*, 2006.
(24) Huber, C.; Wächtershäuser, G. *Science* **1997**, *276*, 245.
(25) Huber, C.; Wächtershäuser, G. *Science* **1998**, *281*, 670.
(26) Huber, C.; Eisenreich, W.; Hecht, S.; Wächtershäuser, G. *Science* **2003**, *301*, 938.
(27) Leman, L.; Orgel, L.; Ghadiri, M. R. *Science* **2004**, *306*, 283.
(28) Cody, G. D.; Boctor, N. Z.; Brandes, J. A.; Filley, T. R.; Hazen, R. M.; Yoder, H. S., Jr. *Geochim. Cosmochim. Acta* **2004**, *68*, 2185.

reactions, that other iron−sulfide phases such as the much more prevalent pyrite, FeS_2, could also serve as catalysts.

A detailed examination, at the molecular level, is now paramount in order to investigate the various chemical reactions involved and to address the role of mineral surfaces as well as other chemical and geophysical prebiotic conditions in the formation of peptides from amino acids. Recent advances in ab initio molecular dynamics (AIMD) computer simulation techniques, in particular Car−Parrinello MD,[29] in conjunction with available computer technology make it possible to study such complex chemical reactions fully "in silico".[30] The first such ab initio molecular dynamics simulation at "ISW conditions" was carried out only recently.[31] Since, in the ISW scenario, it is of crucial importance that metabolites stay at the pyrite surface in order to increase their effective concentrations, the authors focused on glycine adsorption at the pyrite−water interface using an ideal (100) surface of FeS_2. At a temperature of 500 K and an estimated pressure of about 20 MPa, resembling the hydrothermal environment, they found that a glycine molecule, previously adsorbed in a monodentate mode via a carboxylate oxygen, desorbs readily on a picosecond time scale in a water-mediated process. In a follow-up investigation,[32] a bidentate adsorption mode was found to improve the situation somewhat by leading to a longer retention time as compared to the monodentate case. Detailed analyses of the electronic structure in terms of Fukui functions revealed that the iron atoms of the pyrite surface are potential targets for further nucleophilic or electrophilic attacks and thus for chemical reactions, unlike the attached glycine molecule. An important finding of these two studies is that hydrogen bonding of the aqueous environment plays a decisive role in desorption processes of glycine at such a pyrite−water interface. AIMD simulations using a similar setup show that amino acids adsorb weakly at hydroxylated TiO_2 surfaces.[33] To increase the retention time, an anchoring group like carbonyl sulfide attached to glycine or the presence of surface defects, as suggested by Wächtershäuser,[34] seems to be required. The present paper addresses the latter point in detail. We note in passing that these investigations not only are interesting in the framework of the "origin of life" research but also contribute to the novel organic chemistry in sub- or supercritical water. This field obtained much attention recently as hot pressurized water not only leads to different relative solvation free energies of polar/nonpolar and zwitterionic/neutral solutes in comparison to water at ambient conditions but also reacts differently with organic molecules and allows for noncatalytic chemical reactions under appropriate extreme thermodynamic conditions.[35,36]

Iron pyrite, also known as "Fool's Gold", is an abundant sulfide mineral in the earth's crust. Due to its importance in other fields, detailed investigations of the highly exposed (100) FeS_2 surface of pyrite were performed using various experimental characterization techniques such as X-ray photoelectron spectroscopy (XPS),[37−39] scanning tunneling microscopy (STM),[40,41] low energy electron diffraction (LEED),[41] and electron energy-loss spectroscopy (EELS).[42] Theoretical investigations not only helped to understand the electronic structure of the bulk pyrite and different surfaces[39,43−51] but also elucidated the adsorption of various small molecules.[52−55] Importantly, the high reactivity of naturally occurring pyrite is thought to be due to a typically high concentration of sulfur vacancies on the fractured (100) surface.[37,56,57] Using a combination of experimental and theoretical techniques to characterize the structure of defects at the pyrite (100) surface, it was found[58] that apart from steps and terraces the most prominent type of defects on the fractured surface are sulfur vacancies. Undercoordinated iron atoms resulting from such point defects are expected to bind carboxylate oxygen atoms of glycine stronger compared to iron at an ideal surface and therefore to increase the retention time of glycine.

The purpose of this study is to investigate the possible role of surface sulfur vacancies in stabilizing adsorbed amino acids at pyrite−water interfaces under ISW conditions to allow for further reactions to occur. After examining the impact of the formation of sulfur vacancies on the electronic structure as such, we turn our attention to different adsorption modes of water and glycine at such a defect site. Furthermore, the metadynamics sampling technique[59] in its extended Lagrangian formulation[60,61] is employed in conjunction with Car−Parrinello ab initio molecular dynamics[29,30] to efficiently explore the desorption mechanism, to estimate the relative free energy differences of the various free energy minima together with the connecting free energy barriers along preferred paths, and finally to estimate approximate retention times of glycine on defective pyrite−water interfaces.

2. Methods and Models

The calculations were performed within the Kohn−Sham density functional theory in its plane wave/pseudopotential formulation. The PBE[62] exchange-correlation functional was chosen, and the core

(29) Car, R.; Parrinello, M. *Phys. Rev. Lett.* **1985**, *55*, 2471.
(30) Marx, D.; Hutter, J. In *Modern Methods and Algorithms of Quantum Chemistry*; NIC, FZ Jülich, 2000. For downloads see http://www.theochem-.rub.de/go/cprev.html.
(31) Boehme, C.; Marx, D. *J. Am. Chem. Soc.* **2003**, *125*, 13362.
(32) Pollet, R.; Boehme, C.; Marx, D. *Origins Life Evol. Biospheres* **2006**, http://dx.doi.org/10.1007/s11084-006-9010-0.
(33) Langel, W.; Menken, L. *Surf. Sci.* **2003**, *538*, 1.
(34) Wächtershäuser, G. Private communication.
(35) Nagai, Y.; Morooka, S.; Matubayasi, N.; Nakahara, M. *J. Phys. Chem. A* **2004**, *108*, 11635.
(36) Weingärtner, H.; Frank, E. U. *Angew. Chem., Int. Ed.* **2005**, *44*, 2672.
(37) Nesbitt, H. W.; Bancroft, G. M.; Pratt, A. R.; Scaini, M. J. *Am. Mineral.* **1998**, *83*, 1067.
(38) Guevremont, J. M.; Elsetinow, A. R.; Strongin, D. R.; Bebie, J.; Schoonen, M. A. A. *Am. Mineral.* **1998**, *83*, 1353.
(39) von Oertzen, G. U.; Skinner, W. M.; Nesbitt, H. W. *Phys. Rev. B* **2005**, *72*, 235427.
(40) Eggleston, C. M.; Ehrhardt, J.-J.; Stumm, W. *Am. Mineral.* **1996**, *81*, 1036.
(41) Rosso, K. M.; Becker, U.; Hochella M. F., Jr. *Am. Mineral.* **1999**, *84*, 1535.
(42) Garvie, L. A. J.; Buseck, P. R. *Am. Mineral.* **2004**, *89*, 485.
(43) Zeng, Y.; Holzwarth, N. A. W. *Phys. Rev. B* **1994**, *50*, 8214.
(44) Eyert, V.; Höck, K.-H.; Fiechter, S.; Tributsch, H. *Phys. Rev. B* **1998**, *57*, 6350.
(45) Opahle, I.; Koepernik, K.; Eschrig, H. *Phys. Rev. B* **1999**, *60*, 14035.
(46) Gerson, A. R.; Bredow, T. *Surf. Interface Anal.* **2000**, *29*, 145.
(47) de Leeuw, N. H.; Parker, S. C.; Sithole, H. M.; Ngoepe, P. E. *J. Phys. Chem. B* **2000**, *104*, 7969.
(48) Muscat, J.; Hung, A.; Russo, S.; Yarovsky, I. *Phys. Rev. B* **2002**, *65*, 054107.
(49) Hung, A.; Muscat, J.; Yarovsky, I.; Russo, S. P. *Surf. Sci.* **2002**, *513*, 511.
(50) Guanzhou, Q.; Qi, X.; Yuehua, H. *Comput. Mater. Sci.* **2004**, *29*, 89.
(51) Cai, J.; Philpott, M. R. *Comput. Mater. Sci.* **2004**, *30*, 358.
(52) Stirling, A.; Bernasconi, M.; Parrinello, M. *J. Chem. Phys* **2003**, *118*, 8917.
(53) Stirling, A.; Bernasconi, M.; Parrinello, M. *J. Chem. Phys* **2003**, *119*, 4934.
(54) Hung, A.; Yarovsky, I.; Russo, S. P. *J. Chem. Phys* **2003**, *118*, 6022.
(55) Philpott, M. R.; Goliney, I. Y.; Tin, T. T. *J. Chem. Phys* **2004**, *120*, 1943.
(56) Luck, J.; Hartmann, A.; Fiechter, S. *Z. Anal. Chem.* **1989**, *334*, 441.
(57) Birkholz, M.; Fiechter, S.; Hartmann, A.; Tributsch, H. *Phys. Rev. B* **1991**, *43*, 11926.
(58) Andersson, K.; Nyberg, M.; Ogasawara, H.; Nordlund, D.; Kendelewicz, T.; Doyle, C. S.; Brown, G. E., Jr.; Pettersson, L. G. M.; Nilsson, A. *Phys. Rev. B* **2004**, *70*, 195404.
(59) Laio, A.; Parrinello, M. *Proc. Natl. Acad. Sci.* **2002**, *99*, 12562.
(60) Iannuzzi, M.; Laio, A.; Parrinello, M. *Phys. Rev. Lett.* **2003**, *90*, 238302.
(61) Ensing, B.; Vivo, M. D.; Liu, Z.; Moore, P.; Klein, M. L. *Acc. Chem. Res.* **2006**, *39*, 73.

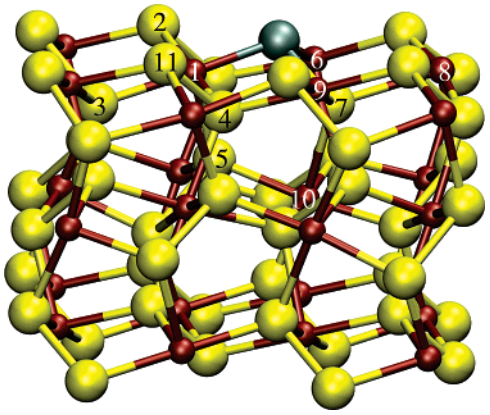

Figure 1. Relaxed pyrite slab, $Fe_{24}S_{47}$, used to represent the (001) FeS_2 surface; the gray sphere represents the sulfur atom removed from the ideal surface to create the surface sulfur vacancy defect; yellow and brown spheres represent sulfur and iron atoms, respectively.

electrons were taken into account using the Vanderbilt's ultrasoft pseudopotentials[63] containing additional *d*-projectors in case of sulfur as well as scalar relativistic corrections and semicore states for iron. For the set of used ultrasoft pseudopotentials, a plane wave cutoff of 25 Ry was sufficient to obtain convergence in the unit cell parameter and the sulfur dimer S−S distance of bulk pyrite; more details of the corresponding benchmark calculations are described in ref 32. Structure relaxation and AIMD simulations were performed using the CPMD package,[30,64] whereas static band structure calculations were done using the PWscf code[65] and identical pseudopotentials. For technical reasons the single-point calculations of the electron localization function (ELF)[66] were performed with Troullier−Martins norm-conserving pseudopotentials[67] along with the BP86 functional[68,69] and a plane wave cutoff of 120 Ry.

The supercell for the present slab calculations was an orthorhombic box having the dimensions 10.808 × 10.808 × 18.914 Å^3 as used before.[31,32] The pyrite slab exposed the (100) surface and was comprised of nine atomic layers with 24 Fe and 48 S atoms in total. A surface sulfur vacancy was introduced by removing a 3-fold coordinated sulfur atom from the top layer of the slab (see Figure 1). Band structure calculations for the ideal and defect surfaces were performed with their energy minimum structures using 4 × 4 × 1 Monkhorst−Pack *k*-point meshes. During both structure relaxations and molecular dynamics simulations, the bottom three atomic layers were kept fixed at their optimized bulk positions. A space of about 10 Å between the top of the slab and its image in the [100] direction contained 35 water molecules plus a glycine molecule. Constant temperature AIMD simulations were performed using the Car−Parrinello scheme[29] along with Nosé−Hoover chain[70] thermostats for nuclei and electronic orbitals. The system was thermostated to 500 K, which results in an expected pressure of about 20 MPa in order to mimic ISW thermodynamic conditions. A time step Δt of 0.144 fs was used for the integration of the equations of motion, the fictitious mass for the orbitals was 700 au, and the hydrogen mass was substituted by the deuterium mass. The starting structures for the AIMD simulations were obtained by the following equilibration protocol. A pre-equilibrated water system was added to a glycine adsorbed on the surface and equilibrated at 500 K for 1 ps, while the atomic positions of the glycine molecule as well as those of the pyrite slab were kept fixed and all remaining dynamical degrees of freedom were thermostated. After releasing the fixed degrees of freedom with the exception of the lowest three atomic layers of the pyrite slab, a trajectory of 7 ps was obtained.

To estimate the free energy barrier for the desorption of glycine we employed the metadynamics technique[59] as reviewed in ref 61. At the core of this method is a coarse-graining of the degrees of freedom thereby reducing the dimensionality of the relevant subspace as much as possible. This is achieved by an appropriate selection of a small set of collective coordinates $\{S_\alpha(\mathbf{R})\}$, which distinguishes reactant and product states and describes the process of interest; these coordinates are usually analytical functions of (a subset of all) nuclear positions $\mathbf{R} = \{\mathbf{R}_I\}$. The continuous extended Lagrangian metadynamics formulation[60] was used for all calculations presented here. In this scheme, a set of classical auxiliary particles, $\{s_\alpha\}$, equal in number to that of the selected collective coordinates N_s, extends the physical degrees of freedom. These particles move with fictitious kinetic energy $\sum_\alpha^{N_s} M_\alpha \dot{s}_\alpha^2/2$ and their motion is coupled to that of the collective coordinates, $\{S_\alpha\}$, by a harmonic potential $\sum_\alpha^{N_s} k_\alpha[S_\alpha(\mathbf{R}) - s_\alpha]^2/2$, therefore restraining the dynamics of the latter.

Here, M_α and k_α are the fictitious mass and coupling constant of the auxiliary coordinate s_α, respectively. To escape from free energy minima in the subspace spanned by $\{S_\alpha\}$ and to eventually map the underlying free energy surface, a repulsive time-dependent potential $V(t,\mathbf{s})$ is slowly built up as the dynamics proceeds. In the present work $V(t,\mathbf{s})$ was chosen to be a spherical Gaussian potential of constant height and width, W and $\Delta s^\perp$, respectively,

$$V(t,\mathbf{s}) = W\sum_{t_i<t} \exp\left\{-\frac{[\mathbf{s}(t) - \mathbf{s}(t_i)]^2}{2(\Delta s^\perp)^2}\right\} \qquad (1)$$

which is dropped at times t_0, t_1,..., t_i.... Thus, this potential is updated at the metadynamics time step, $\Delta t_{meta} = t_{i+1} - t_i$, which is an integer multiple of the AIMD time step Δt.

Having the accumulated information on the positions, widths, and heights of the Gaussians deposited during a metadynamics simulation, reconstruction of the free energy landscape underlying the dynamics is technically straightforward. The (Helmholtz or *NVT*) free energy $F(\mathbf{s})$ can be estimated as

$$F(\mathbf{s}) = -\lim_{t\to\infty} V(t,\mathbf{s}) + \text{constant} \qquad (2)$$

so that relative free energies and free energy barriers can be obtained readily from metadynamics simulations.[59−61] The parameters M_α, k_α, W, $\Delta s^\perp$, and Δt_{meta} were chosen according to earlier experience.[71] They allow the collective coordinate $S_\alpha(\mathbf{R})$ and the associated auxiliary variable s_α to move close to each other, such that the dynamics of the latter maintains adiabatic separation from the electronic degrees of freedom.[72] Moreover, a reasonable sampling of the free energy landscape is obtained in an affordable computational time. In the present investigation only one type of collective coordinates was necessary, namely coordination numbers $S_{A-B(1,...,NB)}(\mathbf{R}) = c[A - B(1,..., N_B)]$ between a particular atom A with respect to a set B(1,..., N_B) of N_B other atoms, which is defined by

$$c[A - B(1,..., N_B)] = \sum_I^{N_B} \frac{1 - (R_{AI}/R_{AB}^0)^6}{1 - (R_{AI}/R_{AB}^0)^{12}} \qquad (3)$$

where $R_{AI} = |\mathbf{R}_A - \mathbf{R}_{BI}|$ denotes the distance between atom A and the I th B atom. For each pair of atoms, this function is nearly unity when

(62) Perdew, J. P.; Burke, K.; Ernzerhof, M. *Phys. Rev. Lett.* **1996**, *77*, 3865. Erratum: *Phys. Rev. Lett.* **1997**, *78*, 1396.
(63) Vanderbilt, D. *Phys. Rev. B* **1990**, *41*, 7892.
(64) *CPMD*, version 3.9.2; IBM Corp. 1990−2006, MPI für Festkörperforschung Stuttgart 1997−2001. See also http://www.cpmd.org.
(65) *PWscf code*, version 2.1.3; in Quantum-ESPRESSO; see also http://www.pwscf.org/, 2006.
(66) Savin, A.; Nesper, R.; Wengert, S.; Fässler, T. F. *Angew. Chem., Int. Ed. Engl.* **1997**, *36*, 1809. See also http://www.cpfs.mpg.de/ELF/.
(67) Troullier, N.; Martins, J. L. *Phys. Rev. B* **1991**, *43*, 1993.
(68) Perdew, J. P. *Phys. Rev. B* **1986**, *33*, 8822.
(69) Becke, A. D. *Phys. Rev. A* **1988**, *38*, 3098.
(70) Martyna, G. J.; Klein, M. L.; Tuckerman, M. *J. Chem. Phys.* **1992**, *97*, 2635.
(71) Ensing, B.; Laio, A.; Parrinello, M.; Klein, M. L. *J. Phys. Chem. B* **2005**, *109*, 6676.

the bond distance $R_{AI} < R^0_{AB}$ and is about zero for $R_{AI} > R^0_{AB}$, whereby R^0_{AB} is a cutoff bond distance.

Having mapped such free energy surfaces, $F(\mathbf{s})$, the simplest ansatz conceivable, i.e., the framework of unimolecular reaction dynamics together with transition state theory, can be used to estimate, very roughly, the order of magnitude of the time scales $\tau_{1/2} = \ln 2/k$ on which a process occurs along computed minimum free energy paths. The rate constant k of the rate-determining step along such paths is approximately obtained from

$$k = \frac{k_B T}{h} \exp(-\Delta F^{\ddagger}/k_B T) \quad (4)$$

where $\Delta F^{\ddagger}$ is the largest free activation energy barrier involved.

3. Results and Discussion

3.1. Sulfur Vacancy: Relaxation Effects and Electronic Structure. In this section the impact on the geometric and electronic structure of the ideal and clean pyrite (100) surface upon creating a surface sulfur vacancy is discussed. In bulk pyrite, iron atoms are octahedrally coordinated by six sulfur atoms and each sulfur atom is tetrahedrally bonded to one sulfur, thus forming a sulfur dimer, and three iron atoms. The upper part of the valence band mostly consists of iron t_{2g} (i.e., d_{xy}, d_{xz}, and d_{yz}) orbitals which are nonbonding according to crystal field theory.[73] The lower part of the conduction band has contributions from iron e_g (i.e., d_{z^2} and $d_{x^2-y^2}$) and sulfur p states; see refs 41, 44, and 73 for more details. By the formation of the (100) surface, one Fe−S bond of every iron and sulfur atom at the surface is broken. This results in 5-fold coordinated iron atoms at the surface, therefore lifting the octahedral symmetry and thus the degeneracy within the t_{2g} and e_g manifolds.

While the creation of an ideal (100) pyrite surface keeps the sulfur dimers intact, they are locally destroyed by the generation of sulfur vacancies on this pyrite face. In our special case with one sulfur vacancy, the sulfur atom S(7) is therefore 3-fold coordinated and the two iron atoms Fe(1) and Fe(6) are 4-fold coordinated (see Figure 1 for labeling scheme). As each sulfur atom has a formal charge of −1, formation of a sulfur vacancy by the removal of a neutral sulfur atom will leave this charge in the system to maintain charge neutrality. It has been suggested[57] that the sulfur atom, which was once the part of the sulfur dimer, becomes S^{2-} as a result of the formation of a sulfur vacancy. Accordingly, this sulfur atom remains in tetrahedral coordination with the lone pair of electrons directed to an apex of the tetrahedron. Additional evidence for the localization of the extra electron comes from XPS spectroscopy of the fractured pyrite (100) surface.[37,58] The authors assigned the signal at 160.95 eV to the S(2p) state of the S^{2-} species. To substantiate such a bonding situation, we compare the energies for different spin states of the defective surface. It turns out that within our approach the triplet state is 28 kJ/mol higher in energy compared to the singlet state, which has the same energy in an open and closed shell (i.e., spin-polarized and unpolarized DFT) calculations. This shows that the extra electron created by formation of a sulfur vacancy is indeed paired. To check its arrangement in real space, we have computed the difference in the electron localization function (ELF) of the ideal and defective surfaces, see Figure 2, which exhibits most predominantly the difference in the electron *pair* localization properties.[66] The blue regions in this figure show indeed localization of an electron pair at S(7), which does not exist on the ideal surface. Apart from the green part, which is due to the missing lone pair of the removed sulfur atom and is thus only present on the ideal surface, there is no additional difference of any significance between the ideal and the defective case. In conclusion, these analyses confirm the earlier presumption[57] that the electron remaining at this surface, upon removal of one sulfur atom, localizes at sulfur S(7), which then formally becomes S^{2-}, and forms a lone electron pair pointing toward the vacancy.

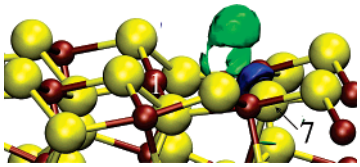

Figure 2. Difference of the ELF (at an isosurface value of 0.8) for the ideal and defective surface along with part of the slab used for the defect calculation. The corresponding contributions represented in green and blue color are present in the defective and ideal cases, respectively.

Table 1. Relaxations of Selected Bond Distances (Å) Neighboring the Defect Site; See Figure 1 for Atom Labeling Scheme

	bond distance		
bond	ideal	defect	relaxation
Fe(1)−S(2)	2.248	2.250	0.002
Fe(1)−S(3)	2.261	2.192	−0.069
Fe(1)−S(4)	2.246	2.212	−0.034
Fe(1)−S(5)	2.129	2.125	−0.004
S(7)−Fe(8)	2.264	2.371	0.107
S(7)−Fe(9)	2.245	2.290	0.045
S(7)−Fe(10)	2.319	2.452	0.133

To investigate structural perturbations due to this sulfur vacancy, we compare the relaxed ideal and defective slabs in Table 1. Major structural changes occurred around the defect site. While almost all bonds formed by Fe(1) become shorter, all bond distances to S(7) are found to increase due to defect formation. The relaxation of bonds to Fe(6) are similar to that of Fe(1) and therefore not listed in Table 1. The sulfur atom S(7) moved about 0.10, 0.17, and 0.22 Å along the *x*, *y*, and *z* axes, respectively; i.e., it is found to shift toward the defect site. Apparently this is the consequence of distortion in the tetrahedral environment of S(7) as a result of the creation of a localized lone pair. The displacement of this sulfur atom is in qualitative agreement with earlier calculations.[58]

Apart from these structural ramifications, the formation of this surface point defect causes a reordering in the d orbitals of the two iron atoms Fe(1) and Fe(6). According to crystal field theory, removing a sulfur atom along the *x*-axis will lower the energies of d_{xz} and d_{xy} states in the upper part of the valence band and the $d_{x^2-y^2}$ in the lower part of the conduction band. In Figure 3 we compare the projected density of states (PDOS) for the t_{2g} and e_g orbitals of all iron atoms and the p orbitals of all sulfur atoms in the system for the ideal (Figure 3a) and defective (Figure 3b) surfaces. The set of states between −1.5

(72) We used k_α and M_α equal to 2.0 au (5252 kJ/mol) and 50 amu (91 144 au), respectively, for all calculations. The (dimensionless) Gaussian width Δs^1 was 0.05, and the height W was varied between roughly 1 and 10 kJ/mol. An adaptive metadynamics time step Δt_{meta} was used in such a way that a new Gaussian is placed only if the collective variables have moved by $3\Delta s^1/2$, and this occurred typically between 50 and 250 MD time steps Δt in our simulations. For the starting structure depicted in Figure 5a, the cutoff bond distances $R^0_{N-Fe(1)}$, R^0_{O-Fe}, and R°_{N-H} were 3.0, 3.0, and 1.4 Å, respectively.

(73) Bither, T. A.; Bouchard, R. J.; Cloud, W. H.; Donohue, P. C.; Siemons, W. J. *Inorg. Chem.* **1968**, *7*, 2208.

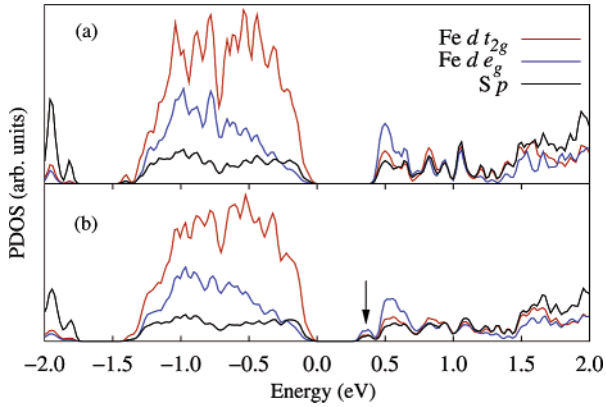

Figure 3. Projected density of states (PDOS) of the sulfur p and iron t_{2g} and e_g sets of orbitals for the ideal (a) and the defective (b) pyrite (100) surface with their Fermi levels shifted to 0 eV; the state created in the gap by the point defect is marked by an arrow in (b); a Gaussian broadening with a width of 0.03 eV was used.

and 0 eV, which is the upper level of the valence band, is mostly populated with t_{2g} states as expected from the crystal field theory.[73] In addition to that, there are still significant contributions from Fe e_g as well as from S p orbitals, which is in accordance with reported observation.[41] Overall, there is no qualitative difference between the ideal and defective surfaces *below* the Fermi level. The conduction band of the ideal slab starts at about 0.40 eV, and its lower part is largely populated with e_g states along with about equal contributions from t_{2g} and S p states. Interestingly, for the defect case, a new set of states appears in the band gap region of the ideal slab, which is highlighted by an arrow in Figure 3b for clarity. These defect states not only consist of t_{2g} orbitals as predicted by the crystal field theory but also include appreciable contributions from Fe e_g and S p states. This novel defect state is located between 0.27 and 0.40 eV, thereby lowering the band gap from 0.40 to 0.27 eV; note that the PDOS is converged with respect to *k*-point sampling. Although it is known that the band gap of the naturally occurring pyrite surfaces (about 0.2 eV) is lower than that of ideal bulk (0.95 eV)[40] due to the presence of defects, more precise experiments on the effect of the sulfur vacancy in the electronic structure of pyrite do not exist to our knowledge. Overall in our calculations, the band gap decreases from 0.87 to 0.4 to 0.27 eV by changing from bulk to ideal surface to defective surface. Due to their lower coordination number, the iron atoms neighboring the vacancy are expected to be more reactive compared to those of the ideal surface. In particular, considering the large contributions of the d_{z^2} state in the lowest conduction band region, which should be much more pronounced in comparison to the ideal slab,[32] nucleophilic reactants should prefer to attack these Fe atoms in an almost perpendicular direction to the surface In addition to that, it can be judged on the basis of the presence of both iron $d_{x^2-y^2}$ and sulfur p orbitals in the defect state, which are oriented toward the defect site, that the two 4-fold coordinated iron and 3-fold coordinated sulfur atoms near a surface vacancy can bind the adsorbates at this point defect. Overall, the electronic structure analysis strongly suggests the way in which the surface with sulfur vacancies is more reactive than the ideal surface.

3.2. Water Adsorption at the Sulfur Vacancy. Having investigated structural and electronic relaxations due to the formation of a sulfur vacancy, the attention is now turned to

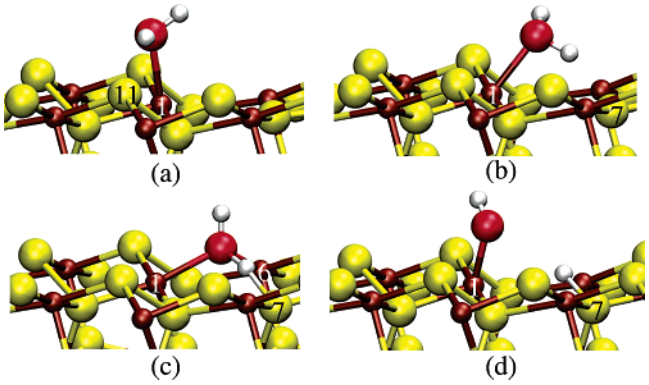

Figure 4. Important molecular (upper row) and dissociative (lower row) adsorption modes of a single water molecule at the sulfur vacancy on the pyrite (100) surface; red and white spheres represent oxygen and hydrogen atoms, respectively, and see Supporting Information for energies and coordinates.

Table 2. Adsorption Energies (E_{ads}) of a Single Water Molecule and Relative Energies (E_{rel}) of a Glycine Molecule in the Important Adsorption Modes from Figures 4 and 5, Respectively, on the Pyrite (100) Surface Close to the Surface Sulfur Vacancy[a]

water	E_{ads}	glycine	E_{rel}
Figure 4a	−72	Figure 5a	0
Figure 4b	−58	Figure 5b	59
Figure 4c	−60	Figure 5c	46
Figure 4d	−18	Figure 5d	85

[a] All energies are given in kJ/mol, and E_{rel} is reported with respect to the most favored structure Figure 5a.

the chemical consequences of these changes. Various adsorption modes of one water molecule at the defect site were studied, the four energetically most important ones will be discussed in the following, before proceeding to the glycine adsorption problem. A water molecule was molecularly adsorbed at the 4-fold coordinated iron Fe(1) near the sulfur vacancy in two different ways (see Figure 4a,b). Whereas the water molecule in Figure 4a coordinates a "normal" surface sulfur atom S(11) via its hydrogen atom, in Figure 4b it interacts with the 3-fold coordinated sulfur atom S(7) which is not involved in any S−S bond as a result of the vacancy. The adsorption energy of the structure in Figure 4a is about −72 kJ/mol; see Table 2 for a compilation of these data, which is considerably lower (by about 10 kJ/mol) than that on a defect-free ideal surface; the data of the ideal surface calculated with the electronic structure approach used here compare well to those obtained earlier with a similar but not identical approach[52] as documented in the Supporting Information.[74] This is not a surprising result as we anticipated from the electronic structure analysis in section 3.1 strong bonding along the axial direction, i.e., nearly normal to the surface, taking into account a high d_{z^2} state density in the lower part of the conduction band. An additional short (about 2 ps) AIMD run for the structure depicted in Figure 4a at 300 K did not reveal any appreciable structural changes. The second molecular adsorption mode shown in Figure 4b is less favored by about 14 kJ/mol (see Table 2).

It has been reported[52] that on the ideal (100) surface dissociative adsorption of water should not be expected due to positive adsorption energies E_{ads}, which is also supported by

(74) Adsorption energies of both the molecular and dissociative adsorption modes of water on the ideal (100) FeS_2 surface are provided in the Supporting Information.

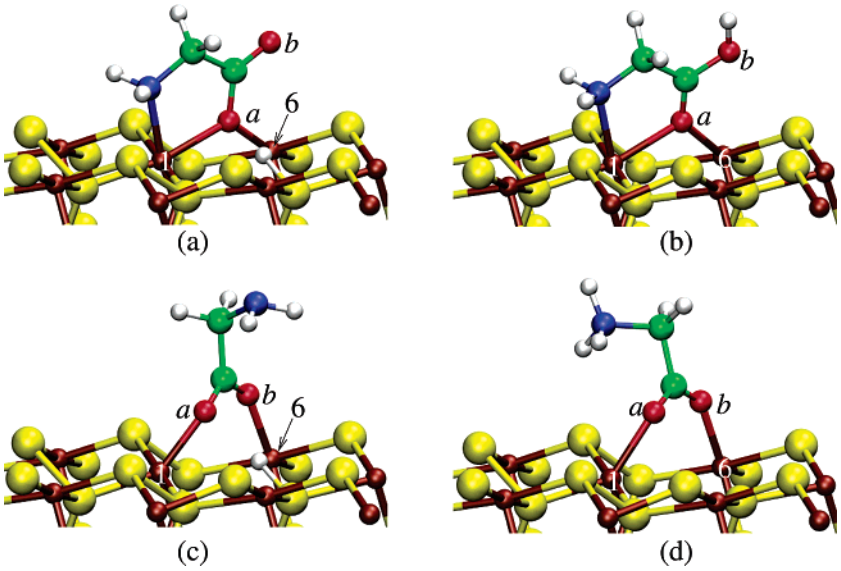

Figure 5. Important cyclic (upper row) and zwitterionic (lower row) adsorption modes of a glycine molecule at the sulfur vacancy on the pyrite (100) surface; blue and green spheres represent nitrogen and carbon atoms, respectively, and see Supporting Information for energies and coordinates.

the present calculations using the defect-free surface.[74] To scrutinize whether the presence of an isolated surface vacancy might change the picture by allowing for dissociative adsorption, we took two additional, nonmolecular adsorption configurations into account. The first configuration represents a "partially dissociated" water molecule at the defect site and is shown in Figure 4c. Indeed, the absorption energy is found to be negative so that dissociative adsorption can occur due to the presence of the point defect, contrary to the ideal surface case.[52] Still, it is about 12 kJ/mol less favorable (see Table 2) compared to the most favored molecular adsorption mode but quite comparable to the second molecular arrangement in Figure 4b. In the partially dissociated structure of Figure 4c, the oxygen atom of the water molecule binds to both 4-fold coordinated iron atoms, Fe(1) and Fe(6), while one of the hydrogen atoms of the water molecule forms a weak bond with the 3-fold coordinated sulfur atom S(7). The optimized S−H and O−H bond distances are found to be 1.56 and 1.21 Å, respectively, the latter being unexpectedly long for a standard covalent O−H bond. Interestingly, a short (about 2 ps) AIMD run at 300 K starting from the optimized structure of Figure 4c revealed that the proton is dynamically shuttling back and forth between the oxygen and the sulfur atom, whereas no other structural changes were observed on this time scale. Thereby, the bond distances vary between about 1.05 and 1.45 Å for the O−H and 1.45 and 1.80 Å for the S−H bond, indicating that the activation barrier for water dissociation and reformation is at most of the order of k_BT (≈2.5 kJ/mol at 300 K). A similar dynamical behavior was observed recently in the case of water adsorption on the ZnO-$(10\bar{1}0)$ surface[75] where it led to the formation of a partially dissociated superstructure.

The fourth configuration to be discussed here represents a "fully dissociated" water molecule at the defect site and is shown in Figure 4d. Compared to the partially dissociated structure in Figure 4c, the Fe−O bond is again axial and one of the hydrogen atoms binds to the 3-fold coordinated sulfur atom S(7). The adsorption energy is only −18 kJ/mol, so that this fully dissociated arrangement should be much less favored than the partially dissociated configuration in Figure 4c and even more so in comparison to the molecular adsorption. However, the results in this section show that the process of dissociative adsorption of isolated water molecules on pyrite, which clearly is an endothermic process on the ideal (100) surface,[52] becomes exothermic in the presence of sulfur vacancies, but molecular adsorption still remains the favored process (see Table 2). This is consistent with the experimental finding that a small amount of dissociated water molecules was observed on the pyrite surface and found to desorb at 400 K via association.[76] These chemical findings underpin the inference of different reactivities of ideal and defective pyrite surfaces as derived from the electronic structure considerations in section 3.1.

3.3. Glycine Adsorption at the Sulfur Vacancy. After having explored various adsorption modes of a single water molecule in section 3.2, we now consider the adsorption of glycine close to the point defect. Among a multitude of studied configurations, only the four energetically most favorable ones are pictured in Figure 5. In the structure from Figure 5a, the iron atom Fe(1) near the defect site is coordinated axially by the nitrogen atom and equatorially by one of the carboxyl oxygen atoms O(*a*) of the glycine molecule. Thus the octahedral environment of iron, as in bulk pyrite, is approximately restored. The same oxygen atom additionally interacts with Fe(6), which also neighbors the sulfur vacancy. The hydrogen atom from the carboxyl group of the glycine molecule is bound to the surface sulfur atom S(7). Thus, this structure corresponds to the adsorption of a zwitterionic glycine molecule at the defect site in a dissociative manner. The adsorption energy is dramatically lower (by about 133 kJ/mol) than that for the zwitterionic monodentate mode on the ideal surface studied earlier.[31] The second structure, depicted in Figure 5b, is very similar to that from Figure 5a, except that the hydrogen atom that was on the surface at the sulfur atom S(7) is now bonded to the free carboxylate oxygen atom, O(*b*). Our calculations show that the structure from Figure 5b is about 59 kJ/mol higher in energy compared to our lowest-energy structure depicted in Figure 5a;

(75) Dulub, O.; Meyer, B.; Diebold, U. *Phys. Rev. Lett.* **2005**, *95*, 136101.

(76) Guevremont, J. M.; Strongin, D. R.; Schoonen, M. A. A. *Am. Mineral.* **1998**, *83*, 1246.

see Table 2 for a compilation of the glycine adsorption energies relative to that energy. Both these structures feature an adsorption pattern where one of the two carboxyl(ate) oxygen atoms, O(*a*), is found to be attached to the surface atoms, whereas O(*b*) points away from the surface. These structures are also cyclic in view of the additional surface contact due to the amino group.

The next candidate found displays an adsorption mode similar to the one considered earlier on the ideal surface,[32] except for the fact that one of the hydrogen atoms of the $-NH_3^+$ moiety has been transferred to sulfur atom S(7), which is nearest to the defect site (see Figure 5c). In this structure, the stabilizing surface contacts due to the amino group, $-NH_2$ or $-NH_3^+$, found in the cyclic situations in Figure 5a and 5b must be given up in order to allow the stabilizing chemical contact of the second oxygen atom to the surface. Compared to the most favored structure from Figure 5a, this configuration is about 46 kJ/mol higher in energy. As we are interested in the glycine adsorption and possible desorption at the pyrite−water interface, we have additionally considered a zwitterionic form of glycine, akin to that studied in the desorption from ideal pyrite.[32] This structure shown in Figure 5d is much higher in energy (by about 85 kJ/mol) compared to the best structure depicted in Figure 5a. Nevertheless, the adsorption energy of this structure is about 48 kJ/mol lower compared to the monodentate zwitterionic on the nondefective ideal surface.[31] In summary, the point defect created by a sulfur vacancy is shown to greatly stabilize both cyclic and zwitterionic adsorption of glycine on the ideal FeS_2-(100) surface, the cyclic mode depicted in Figure 5a being, by far, the most preferred one.

3.4. Glycine at the Defective Pyrite−Water Interface. Based on the exploration and optimization of the most important adsorption structures at the pyrite−vacuum interface in the presence of a sulfur vacancy in section 3.3, we can now continue to investigate glycine on defective pyrite in the presence of hot pressurized water at ISW conditions by AIMD. From the set of optimized structures in Figure 5 we have chosen those in Figure 5a and 5d, being the two extreme limits and representing at the same time cyclic and zwitterionic adsorption, as starting structures to conduct two independent AIMD simulations. The former is the most stable structure of glycine on pyrite in contact with a vacuum, and the latter zwitterionic form is expected to be a reasonable structure in the presence of a high dielectric such as water. Based on these adsorption modes the full pyrite−water interfaces were constructed using the protocol outlined in section 2.

First, we consider the cyclic adsorption mode depicted in Figure 5a. The Fe(1)−N distance (not shown) was found to oscillate continuously around 2.1 Å, showing that glycine has no tendency to detach from the surface during the entire simulation time in the canonical ensemble (see Figure 5a for the labeling of atoms). Displacements of up to about 3 Å were observed for the Fe(1)−O(*a*) distance but the oxygen atom returned on the time scale of less than half a picosecond to the average value of 2.2 Å. Such large fluctuations did not occur for the Fe(6)−O(*a*) distance, which points to a stiffer bonding situation in this case. This dynamically stable behavior is in stark contrast to that observed in the previous studies[31,32] of zwitterionic glycine on the nondefective surface in a monodentate adsorption mode. There, desorption occurred readily, i.e., within 1.5 ps, in a process that was mediated by the transient formation of stabilizing hydrogen bonds with solvation water. Also in the case of a bidentate adsorption mode on the ideal surface the authors observed temporary water-mediated partial detachment of glycine.[32] In the present case the oxygen O(*a*) is located at the vacancy site in the structure in Figure 5a, thus almost being screened from the water molecules. Although the amino group featured donated hydrogen bonds to solvation water throughout the entire simulation, the Fe(1)−N surface contact turned out to be dynamically very stable. An explanation for this strong coordination is provided by the favorable interaction of the nitrogen lone pair with the iron e_g orbitals. Simultaneously this also accounts for the lack of accepted hydrogen bonds by the amino group from solvation water. These results indicate that the adsorption of a glycine molecule is highly stabilized at such a point defect site due to both strong bonding of the amino group to surface iron atoms and the formation of a structure where one of the carboxyl oxygen atoms is efficiently screened from the aqueous solution by being pulled down into the sulfur vacancy.

The calculations for the zwitterionic form from Figure 5d were carried out following the same simulation protocol as that described above. Again, no desorption of this zwitterionic structure was observed on the time scale of the entire simulation. In the initial configuration there was a hydrogen bond between the ammonium group and the surface sulfur atom S(2). This bond was broken within the first few steps of the simulation, and the ammonium group formed an intramolecular hydrogen bond with the neighboring oxygen O(*a*) of the deprotonated carboxylate group, which was stable throughout the rest of the simulation. It should be noted that this adsorption mode is qualitatively similar to the one determined previously for bidentate adsorption of glycine on the ideal surface.[32] Both Fe−O distances never exceeded 2.7 Å which is lower than the reported values on the ideal pyrite surface,[32] where more pronounced fluctuations leading even to temporary water-mediated detachments of one of the carboxylate oxygen atoms from the surface were observed. Although, in the current simulation, hydrogen bonds between water molecules and the oxygen atoms of glycine occurred, they did not cause or mediate desorption. Overall, glycine is much more strongly adsorbed at the sulfur vacancy site compared to the ideal surface, both being in contact with hot pressurized water, which is a result of strong Fe−O coordination at the point defect.

3.5. Glycine Desorption: Mechanisms and Free Energies. 3.5.1. Cyclic Adsorption. In the previous section it has been demonstrated that sulfur vacancy defects, which are characteristic to naturally occurring pyrite surfaces, greatly stabilize glycine at the pyrite−water interface under ISW conditions. The next question that arises in the context of prebiotic chemistry occurring on wet mineral surfaces is to what extent this happens; i.e., what are the pathways and barriers to desorption taking into account solvation and finite-temperature effects at the appropriate thermodynamic conditions? To answer this question in terms of free energy landscapes and retention times, and to investigate the underlying desorption mechanism in pertinent detail, we employed metadynamics AIMD to enforce the desorption process. This method is ideally suited to accelerate processes that occur on time scales that are much beyond those that are accessible with the dynamical simulation method used, which is here Car−Parrinello AIMD, without biasing the system too much.[59−61]

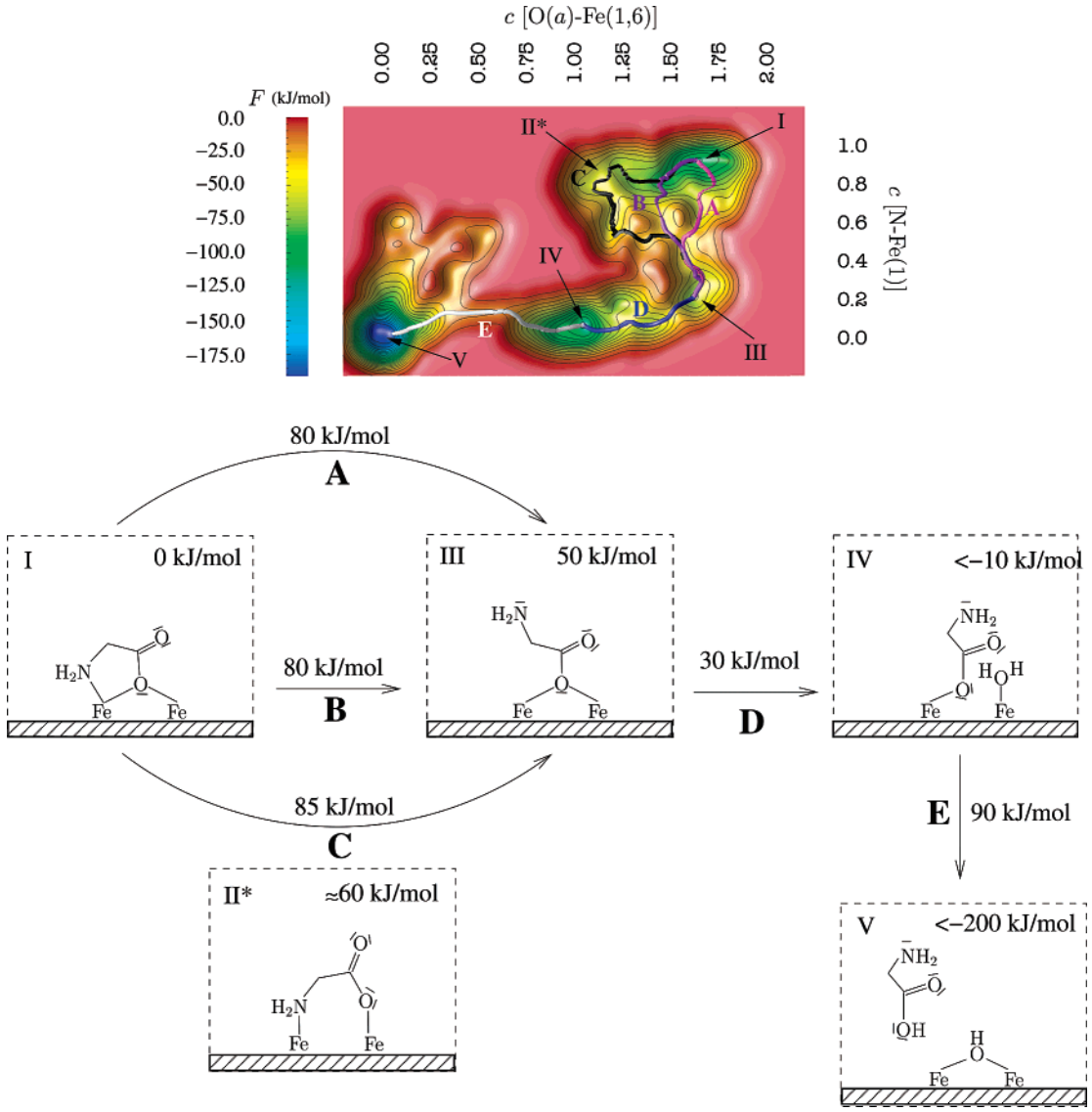

Figure 6. Free energy surface (top) and corresponding schematic mechanism (bottom) for the desorption process of glycine in the cyclic adsorption mode according to Figure 5a at a sulfur vacancy defect at the $FeS_2(100)$−water interface under ISW conditions; letters and Roman numbers denote paths and minima, respectively, and the numbers given inside the boxes and on the arrows are the associated free energies (relative to the initial state I) and the free energy barriers, respectively.

First, desorption starting from the most stable cyclic adsorption mode (see Figure 5a) was studied. The most prominent differences between the adsorbed and solvated state are the coordination numbers of the nitrogen and oxygen atoms of glycine with respect to the iron atoms of the pyrite surface. Thus it is apparent that a full desorption will cause the coordination numbers c[N−Fe(1)] and c[O(a)−Fe(1, 6)] to decrease from unity and two, respectively, to zero; note that c[O(a)−Fe(1, 6)] involves two iron atoms simultaneously according to eq 3. In addition, the possibility exists, which is very conceivable in aqueous environments, of the formation of a zwitterionic glycine by reprotonation of the nitrogen atom by the proton at sulfur S(7) upon desorption, thus raising the coordination number c[N−H] with respect to that particular hydrogen from zero to unity. To capture the complete desorption process, we have taken these three collective coordinates simultaneously into account in the simulation, thus spanning a three-dimensional free energy subspace to be mapped by metadynamics sampling. However, as it turned out, no remarkable changes occurred along the c[N−H] coordinate during the simulation. Therefore it can safely be omitted in the following discussion, and the desorption can be described within the iron−oxygen and iron−nitrogen coordination numbers only. The reconstructed free energy surface projected onto the plane spanned by the collective coordinates c[N−Fe(1)] and c[O(a)−Fe(1, 6)] is shown in the upper part of Figure 6. Several minima beyond the one that defines the starting structure are readily identified. The structures associated with these minima are sketched very schematically in the lower part of Figure 6. Minimum I represents the initial state which is structurally similar to that in Figure 5a, while minimum V is the final state that can be attributed to the fully desorbed glycine molecule. The desorption process is described by the motion of the system on the free energy surface F(c[N−Fe(1)], c[O(a)−Fe(1, 6)]) from the minimum I to V and is found to consist of three distinct steps.

In the first step the amino group desorbs from the pyrite surface. For this reaction there exist, however, several pathways starting at I that all end up in the local minimum III which is about 50 kJ/mol higher in energy than the former. We found three representative pathways from I to III, labeled A, B, and

C in Figure 6, which all contribute to the same reaction channel. Route A is a direct transition, i.e., without an intermediate state, from minimum I to III, and the activation barrier is about 80 kJ/mol. The other two routes, B and C, are characterized by intermediate structures similar to the one sketched as II* (see lower part of Figure 6), which is about 60 kJ/mol higher in energy compared to I. Here, the O(*a*)−Fe(1) bond is broken while the O(*a*)−Fe(6) and N−Fe(1) coordinations are still maintained. The free energy barrier along route B is almost the same as that for A, about 80 kJ/mol, while the surmounting of the barrier on path C requires 85 kJ/mol, which is only one k_BT more than that for the other two routes. An analysis of the trajectory revealed that along the routes B and C, N−Fe(1) bond breakage occurred in a concerted fashion with the recovery of the O(*a*)−Fe(6) bond. In contrast to that, for path A the detachment of the amino group from the surface occurred by an umbrella inversion at the nitrogen atom. These inversions were observed several times and were either thermally induced or mediated by water molecules. Although the three pathways are characterized by different transition states, they meet in the same channel where the coordination number *c*[N−Fe(1)] is below 0.5. The regions spanning the free energy volume around I, II*, and III were completely filled during metadynamics sampling and revisited by the system several times. Considering the myriad of possible hydrogen-bonding topologies and noting that k_BT is of the order of 5 kJ/mol at 500 K, there exist, most probably, even more such connecting filaments on the very flat part of *free* energy surface that characterizes the first step of the desorption process. However, as these filaments differ only in minute details concerning structure and energetics, it is reasonable to consider them as being equivalent in terms of physical relevance.

The second step in the desorption process is the migration of the system from minimum III to IV along path D, which is connected with a decrease of the *c*[O(*a*)−Fe(1, 6)] value from ∼1.7 to ∼1. This means that in minimum IV the oxygen atom O(*a*) is no longer coordinated to two iron atoms, but only to a single one as sketched in the scheme shown in the lower part of Figure 6. The free energy required for the system to surmount the barrier separating III and IV is about 30 kJ/mol, and the free energy of IV is more than 10 kJ/mol lower than that of I (see below for comments on that upper bound). Note that minimum IV can be associated with a set of structures where the O(*a*)−Fe(6) and N−Fe(1) coordinations are broken, but O(*a*) is still coordinated to Fe(1). Among these, configurations were observed with O(*b*) coordinating either Fe(6) or Fe(1) or being solvated; these structures cannot be resolved within the chosen set of collective coordinates as O(*b*) is not explicitly taken into account. To represent this minimum, the structure with the highest probability weight is shown in the sketch in Figure 6. Note that a water molecule occupies the coordination site at Fe(6) after the breakage of the O(*a*)−Fe(6) bond. In this structure the Fe(1)−O(*a*) arrangement is almost equatorial, and thus the oxygen atom O(*a*) is screened from the water solvent.

The last step leading to full desorption of glycine from the surface is described by the lowest energy path E, which connects minima IV and V, and is characterized by a free energy barrier of ∼90 kJ/mol, which is by far the largest one.[77] This process involves the dissociation of one water molecule which is adsorbed at Fe(6). During the dissociation, one proton is transferred from this water molecule to O(*a*) resulting in a solvated neutral glycine molecule and in a hydroxide ion, OH^-. The latter immediately coordinates to the proton that was attached until that point to the sulfur atom S(7) forming a partially dissociated water molecule adsorbed in the defect site (see Figure 6) in a pattern similar to that depicted in Figure 4c for a single water molecule at the defect. Later this partially dissociated configuration converts to an intact water molecule which stays at Fe(6) and remains hydrogen-bonded to S(7) for the rest of the simulation. Note that, in our simulation, we did not attempt to fully map the free energy surface around wells IV and V to economize on simulation time, and thus the absolute values of these free energies relative to minimum I cannot be determined. Nevertheless, one can extract reliable upper bounds of <-10 and <-200 kJ/mol for basins IV and V, respectively, relative to the initial state I.

Remarkably, the desorption process at ISW conditions is found to occur via the formation of a *neutral* glycine molecule rather than a zwitterionic form. On the other hand it is well-known that the zwitterionic form is the most stable one in *ambient* liquid water. The *NVT* free energy difference between the two has been computed recently to be about 47 kJ/mol at *ambient* conditions using virtually identical ab initio molecular dynamics methods.[78] The associated additional thermodynamic stabilization is expected to set in on the subpicosecond time scale after the necessary proton transfer,[78] once the detached glycine has diffused sufficiently far from the surface so that it can surround itself with the equilibrium solvation shell. Although this process cannot be described within our setup in view of the inherent size limitation due to the supercell used, it is noted first of all that the extra stabilization gained is much smaller than that gained from the bare detachment of glycine from the surface at ISW conditions. Second, it is noted that an appreciable shift in the relative stability from the zwitterionic to the neutral form of solvated glycine is anticipated at ISW conditions due to the fact that the dielectric constant of water decreases with increasing temperature and pressure.[36] A small dielectric constant implies in general that the solvation of polar and (zwitter-) ionic molecules is expected to be much less favorable compared to that of nonpolar and neutral species, respectively, thus supporting the idea that glycine could indeed desorb directly into a neutral species at ISW conditions.

3.5.2. Zwitterionic Adsorption. For the desorption of the zwitterionic adsorbed state (similar to Figure 5d), the coordination numbers *c*[Fe(1)−O(*a*)] and *c*[Fe(6)−O(*b*)] were chosen as collective coordinates. Thus, the adsorbed and desorbed states are characterized by the values of these coordinates being unity and zero, respectively. Figure 7 shows the reconstructed free energy surface (top) together with the corresponding sketch of the desorption mechanism (bottom). The full desorption consists of successive breaking of the Fe(1)−O(*a*) and Fe(6)−O(*b*) bonds driving the system from the initial free energy minimum I of the adsorbed state to III and subsequently to the desorbed final state IV.

During the breaking of the Fe(1)−O(*a*) bond, the system migrates from minimum I to III along path A (see Figure 7).

(77) The free energy barrier of this rate-determining step from IV to V has been determined by performing refined metadynamics simulations. The accuracy increases upon lowering the Gaussian height parameter *W*, and the barrier is determined to be 105, 88, and 90 kJ/mol using $W \approx 10.5$, 2.5, and 1.3 kJ/mol, respectively, the latter *W* parameter amounting only to about $^1/_4 k_BT$.

(78) Leung, K.; Rempe, S. B. *J. Chem. Phys.* **2005**, *122*, 184506.

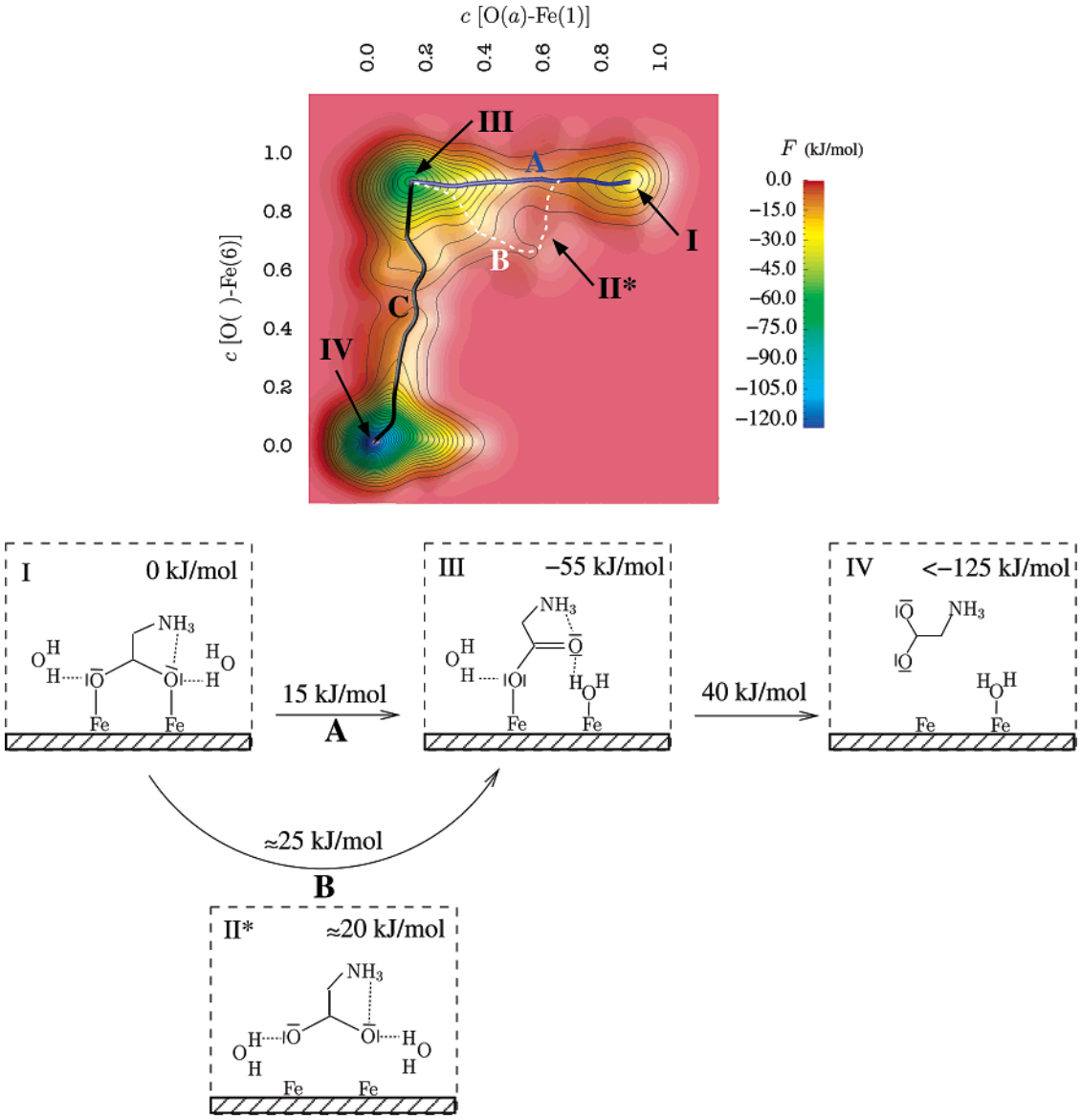

Figure 7. Free energy surface (top) and corresponding schematic mechanism (bottom) for the desorption process of glycine in the zwitterionic adsorption mode according to Figure 5d; see caption of Figure 6 for labeling scheme.

The latter state is 55 kJ/mol lower in energy than the starting structure, and the free energy required for the system to surmount the barrier separating these two minima is about 15 kJ/mol. An analysis of the trajectory shows that the process is mediated by transient hydrogen bonds of O(*a*) to solvation water. After the detachment of O(*a*), the entire glycine molecule reorients around the Fe(6)−O(*b*) bond and a water molecule adsorbs at Fe(1), thus preventing a readsorption of glycine. In addition, the detached glycine oxygen is stabilized by an internal hydrogen bond with the ammonium group as shown schematically in structure III in the lower part of Figure 7. An alternative route exists, connecting basins I and III through a shallow minimum II* (marked route B in the upper part of Figure 7), in which the oxygen atoms O(*a*) and O(*b*) are partially detached from the surface. This process is initialized by the simultaneous hydrogen bonding of two water molecules with O(*a*) and O(*b*). However, this route is less likely compared to route A as the free energy barrier to overcome in this case is about 10 kJ/mol higher.

The subsequent breakage of the Fe−O(*b*) bond along path C, which is the final step of the desorption process, requires a free energy of about 40 kJ/mol.[79] This reaction is also mediated by forming hydrogen bonds to close-by water molecules. Although a complete filling of minimum IV was not achieved in the simulation and thus the exact free energy difference to minimum I cannot be obtained, IV is at least 125 kJ/mol more stable in the sense of a reliable upper bound. The rate-limiting step of the desorption process is the final one, which needs to overcome a barrier of about 40 kJ/mol.

3.5.3. Desorption Time Scales. To summarize, metadynamics simulations starting from two very different starting configurations have shown that desorption from a cyclic adsorption mode of glycine at the defect site on the surface requires more energy to desorb than that from the zwitterionic mode; see Figure 8 for free energies and barriers along the minimum energy paths for the complete desorption process in the case of cyclic and zwitterionic modes. In the cyclic structure, the nitrogen of the

(79) The free energy barrier of this rate-determining step from III to IV has been determined by performing refined metadynamics simulations. The accuracy increases upon lowering the Gaussian height parameter W, and the barrier is determined to be 50 and 40 kJ/mol using $W \approx 5$ and 1.3 kJ/mol, respectively, the latter W parameter amounting only to about $^1/_4 k_B T$.

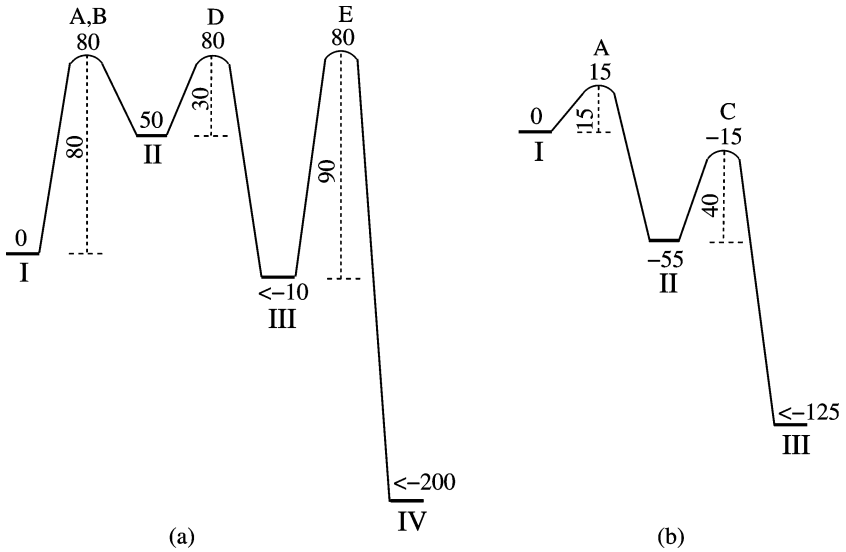

Figure 8. Relative free energies of all minima and saddle points compared with the starting structure plus the free energy barriers (in kJ/mol) for individual processes along the lowest energy paths illustrated in Figures 6 and 7 leading to the complete desorption of glycine from cyclic (a) and zwitterionic (b) adsorption modes are sketched; see Figure 6 and Figure 7 for labeling scheme.

amino group is bonded to a surface iron by donating its lone pair, and thereby no hydrogen bonds exist between this nitrogen atom and the surrounding water, which is unfavorable for detachment to set in. Moreover, in the rate-determining step (see step E in Figure 6 and Figure 8a), the remaining oxygen atom anchored to the surface is bound to an iron atom in such a way that it is geometrically screened from the surrounding water molecules. The possible formation of a zwitterionic form from state III or IV on the free energy surface of Figure 6 would require the dissociation of a water molecule or the desorption of a proton from the surface, such as the one at S(6). Both processes are associated with high free energy barriers. In contrast to that, the zwitterionic structure can desorb assisted by hydrogen-bonding to the solvent molecules, which facilitates the detachment process energetically.

Common to both desorption mechanisms, starting either from the cyclic or from the zwitterionic adsorption mode, is the fact that the highest free energy barrier is surmounted in the very last step of these distinct but complex detachment processes (see Figure 8). The corresponding values of 90 and 40 kJ/mol can roughly be translated into retention times of the order of milliseconds and nanoseconds, respectively, based on the back-of-the-envelope estimate of this time scale according to eq 4. It is worth noting that such desorption occurred on the picosecond time scale at the ideal pyrite−water interface.[31,32] Thus, sulfur vacancies are found to increase the retention time by 3 to 9 orders of magnitude.

4. Conclusions and Outlook

The importance of surface vacancies in stabilizing a glycine molecule at the interface of pyrite, FeS_2(100), with hot compressed water at "Iron Sulfur World" conditions was investigated using ab initio molecular dynamics techniques. It was shown that the formation of such point defects has an appreciable impact on the electronic structure and reactivity of this surface. In particular, the excess electron, due to the breaking of an S−S bond upon sulfur vacancy formation, is localized on the sulfur atom at the vacancy and forms a lone pair pointing toward the defect site; the resulting structural relaxation is weak. Investigation of molecular and dissociative adsorption of isolated water molecules on the pyrite surface indicates that the reactivity of the iron and sulfur atoms is indeed higher around the defect site in comparison to the corresponding ideal nondefective surface. Similarly, preferred adsorption structures of a glycine molecule including neutral and zwitterionic forms have been optimized.

Using two representative but qualitatively different adsorption modes, cyclic and zwitterionic, the mechanisms and free energy barriers for the desorption process at the pyrite−water interface under high temperature and pressure conditions were obtained by employing the metadynamics Car−Parrinello technique. Although the free energy is much lower in the fully solvated (desorbed) state of the glycine molecule, the free energy barriers allowing for desorption are quite high. Compared to the zwitterionic adsorption structure, the activation barrier for the desorption of the cyclic configuration is about two times higher, 105 kJ/mol (noting that $k_BT \approx 4.2$ kJ/mol at 500 K). This difference in the activation barriers can be traced back to the fact that the desorption of the zwitterionic form is mediated by hydrogen-bonding of solvation water with the carboxylate oxygen, which is not possible for the cyclic adsorption structure due to geometric shielding effects. These results indicate that the cyclic adsorption structure, which can only be formed in the presence of surface vacancies, is stable toward desorption on a millisecond scale at the defective pyrite−water interface. The retention time of the zwitterionic configuration is extended from picoseconds on the ideal pyrite−water interface to nanoseconds in the presence of these point defects.

Independent of such details, it can safely be concluded that surface point defects can greatly stabilize adsorbed amino acids at the pyrite−water interface under extreme thermodynamic conditions as proposed in the ''Iron Sulfur World" scenario. Observations made in previous studies that hydrogen-bonding between glycine and water crucially influences the detachment mechanism and thus the retention time of the amino acid due to solvent mediation phenomena are underpinned. However, the sulfur vacancies not only provide strong bonding sites but also structural grooves where an anchor atom, here a carboxylate

oxygen of an amino acid, is geometrically screened from the water thus preventing access of efficient solvent-mediated detachment channels. Naturally occurring pyrite features a large equilibrium concentration of sulfur vacancies at its surfaces. Thus, it is conceivable that it might maintain a sufficiently high concentration of amino acids on its surfaces, which would be a necessary ingredient for any sustained surface chemical reaction on minerals. The next set of questions to be addressed is whether the retention times provided are long enough for further chemical reactions to take place on the surface that would eventually lead to the formation of peptides. Still, desorption must also occur on an appropriate time scale in order to prevent the mineral surface from being "poisoned" by the synthesis products stemming from this two-dimensional chemistry. Work along these directions is in progress in our laboratory.

Acknowledgment. We are grateful to Rodolphe Pollet, Christian Boehme, and Bernd Meyer for fruitful discussions as well as technical help and to Alessandro Laio and Marcella Iannuzzi for sharing their knowledge in using metadynamics. We thank Rechnerverbund-NRW, NIC (Jülich), SSCK (Karlsruhe), and BOVILAB@RUB (Bochum) for providing computational resources, and we gratefully acknowledge DFG (MA 1547/7) and FCI for partial financial support.

Supporting Information Available: Adsorption energies of water on the ideal surface as well as Cartesian coordinates and total Kohn−Sham energies for all structures depicted in Figure 4 and Figure 5. This material is available free of charge via the Internet at http://pubs.acs.org.

JA063295A